

Registration of Multimodal Fluorescein Images Sequence of the Retina

Tae Eun Choe, Isaac Cohen
Institute for Robotics and Intelligent Systems
University of Southern California
tchoe@usc.edu, icohen@usc.edu

Abstract

In this study we present a Y-feature extraction method for registering color and fluorescein angiograms of the retina. The registration of multimodal fluorescein imagery requires the identification of strong geometric features in the retinal images that are invariant across modalities and to temporal grey level variations due to the propagation of the dye in the vessels. The most informative features, invariant across the considered modalities, are the locations of vessels' ramification: the so-called Y-features. We propose a Y-feature extraction method based on the local classification of image gradient information and an articulated model. An appropriate cost function is proposed for fitting the model using a gradient-based approach. The fitted Y-features are subsequently matched across the images for registering the color and fluorescein images. Experimental results obtained on a large database validate the proposed method.

1. Introduction

The diagnosis and quantification of retinal diseases relies on the interpretation of color images and fluorescein angiography image sequences by qualified experts. The fluorescein angiography image sequence depicts the circulation of the sodium fluorescein dye in the retinal vessels and interpreting critical phases in the circulation is a key element for diagnosis. Grey level of the angiograms vary substantially during the circulation of the dye and image sequence as depicted in figure 1, and the geometric registration of the angiograms requires the use of strong geometric invariants. Similarly registering the color image with the acquired angiograms for facilitating the expert's analysis faces similar problems as the grey level are not consistent across modalities. Figure 1 shows various examples of multimodal retinal images.

Several attempts have been made to solve this problem [2]. A common approach in registering multimodal images, especially in medical images, consists in using mutual information [10][14]. This

however, tends to be quite time-consuming and local minima frequently bias the registration process.

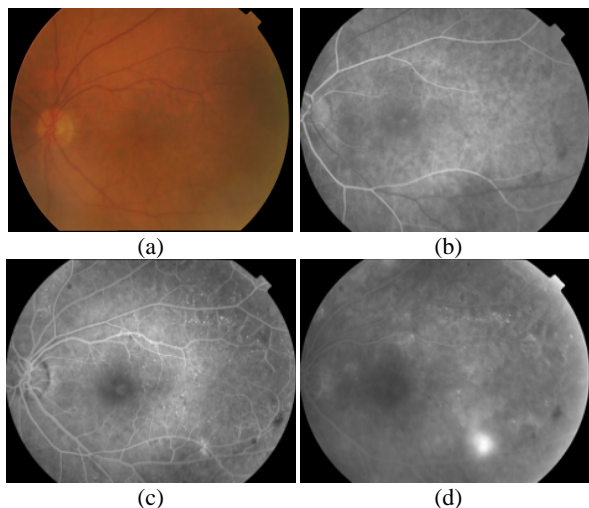


Figure 1. Multimodal Retinal Images

The key element for matching and registering multimodal images is the extraction of invariant geometric features. A commonly used robust feature is the optic disc, where all the vessels and nerves converge. Although many studies [11][15] used the detection of the optic disc for image registration, it is of limited use as it requires the presence of the full optic disc in the images, and assumes that images can be registered by a simple translation model [7]. The latter constitutes a strong limitation when processing real fluorescein angiograms. Vessels constitute important features; however their color, size, and brightness vary across different conditions, and are sometimes impossible to identify in multimodal images due to low contrast. In contrast, Y-features formed by the ramification of vessels provide a reliable feature in retinal image.

Can et al. [3][4][5] presented a method for Y-features detection in retinal images. Y-features are extracted while tracing the vessels by finding the centerline between the left and right boundaries of the vessel. Because the centerline cannot be reliably

extracted in the branch area, this tracing method produces multiple and inaccurate center positions, which subsequently cause errors in image registration. Tsai et al. [13] improved this approach by specifying a branching area and extracting the center position of Y-feature within the area. With this method, the center position is estimated from the closest point of the three linearly approximated traces. Nevertheless, this method still produces multiple Y-features in one branch.

In [17] the authors propose to detect Y-features using mathematical morphology approach with linear elements. This method provides a good detection of bright vessels; for dark vessels, a negative version of the image is used for the morphological process. In transition phases of the circulation of the dye, both dark and bright vessels are present and the proposed method is unable to detect the position of the Y-features accurately.

This paper presents an automatic method for registering color and fluorescein angiograms. The method consists of three main steps: First, seed positions of Y-feature are computed using a PCA-based analysis of directional filters responses. Second, an articulated model of the Y-feature is fitted to the image features using a gradient descent method. Third, the extracted Y-features are matched by maximizing the mutual information, and images are registered using an affine model.

The paper is organized as follows: In section 2 we describe the initial estimation of the position of Y-feature. Section 3 explains the fitting of an articulated Y-feature model and its validation. Section 4 describes the matching of the Y-features and the registration process. Experimental results of these methods are reported and discussed in section 5. Finally, concluding remarks and future research directions are given in Section 6.

2. Estimating Initial Y-feature Positions

In this section, we present a method for locating candidate Y-features in the image. Y-features are characterized by regions in the image where three vessels converge. The position of the Y-feature has at most 3 strong responses from various directional filter output. The PCA based analysis of filter outputs allows locating the position of the Y-feature in the image.

2.1. Directional Filtering

Approximate positions of the Y-features are located using a multiple directional filters. We use a 2-D Laplacian of Gaussian (LoG) filter:

$$LoG = \frac{1}{2\pi\sigma_x\sigma_y} \left(\frac{x^2}{\sigma_x^4} + \frac{y^2}{\sigma_y^4} - \frac{1}{\sigma_x^2} - \frac{1}{\sigma_y^2} \right) e^{-\left(\frac{x}{2\sigma_x^2} + \frac{y}{2\sigma_y^2} \right)} \quad (1)$$

With the proper selection of σ_x and σ_y , elongated shape of the LoG filter is created. With this base kernel, directional filters are formulated by rotating the kernel from 0 to 180 degrees. A large number of directional filters will generate finer responses from the Y-features in the image. However, this can cause duplication of the responses from one vessel. On the other hand, a small number of filters could miss some vessels in the image. We use 6 directional filters with angles of 0, 30, 60, 90, 120, and 150 degree. Figure 2 shows the 6 filters used.

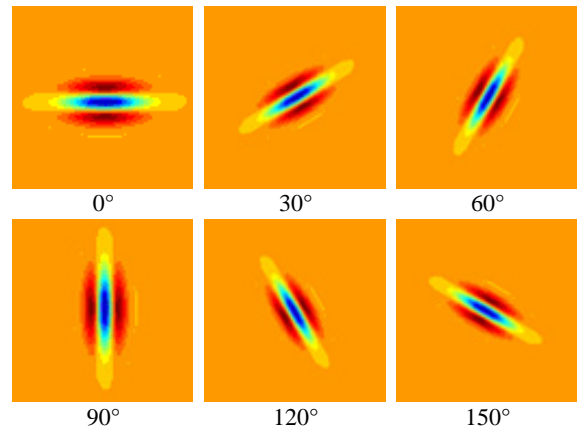


Figure 2. 6 Directional LoG Filters defined using $\sigma_x = 16$ and $\sigma_y = 4$

2.2. Principal Components Analysis

The initial position of Y-features is estimated from the filter output. Since a Y-feature has, at most, 3 different directions, we have used Principal Components Analysis (PCA) method for detecting the pixels with large response from at least 3 filter outputs. A local analysis of the directional filter responses permits integrating responses from neighboring pixels. The obtained 6x6 autocorrelation matrix is analyzed using Singular Value Decomposition (SVD) method. Pixels where three or more eigenvalues are non zero are considered as good a candidate region for a Y-feature.

3. Fitting Articulated Y-feature Model

We propose a Y-feature extraction method based on the fitting of an articulated model. The articulated model is fitted by maximizing the local intensities inside the template and gradient information on the boundary of the template.

3.1. Articulated Model for Y-features

The considered articulated model for the Y-features has 8 DOF, $\mathbf{x} = (x, y, \theta_1, \theta_2, \theta_3, w_1, w_2, w_3)$ which include the center position, three angles, and three widths for each branch. The length of each branch is fixed.

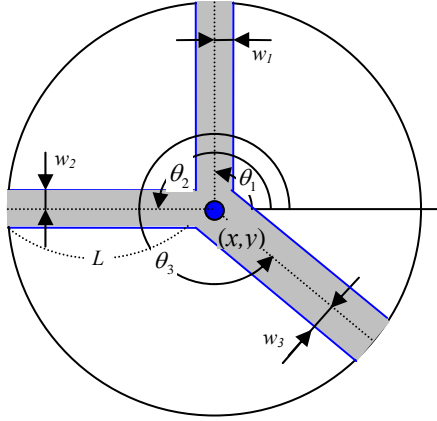


Figure 3. Articulated model of a Y-feature

The three arms rotate, and are attached to the center position. Using the geometric properties of the Y-features in the retinal images, we constrain the arms to be not too close or too far away from each other. The width of each arm is the distance between the center of the vessel to its boundary. More specifically, twice of the width is the actual width of the vessel. The width is also limited to be between the minimum and maximal size of the vessels we are interested in detecting.

3.2. Initialization of Y-feature Shape

Given the seed points extracted by the PCA analysis of the response of the directional filter, the initial orientations of the three arms of the model need to be estimated. Can et al. [3] propose the use of a rectangular grid, and locally detect the maximum intensities for each vertical and horizontal line over the whole image. This however requires dealing with a large number of grids, Y-features located at the edges of the grid cannot be detected and finally the selection of local maximum from four grid line is combined in an *ad-hoc* manner into three best vessels. Our method detects three bright or dark vessels from the circular boundary of Y-feature located on the seed points. Along the circle, peaks or valleys of intensities are detected. Peaks represent bright vessels and valleys correspond to dark vessels. For each peak or valley, the best three arms are selected based on the following error function:

$$F_l(\mathbf{x}) = \frac{1}{2} \sum_{i=1}^3 \int_{-W}^W \int_0^L [I(x_i, y_i, w)]^2 dl dw \quad (2)$$

where L is the length of the branch, W is the width of the branch, i is the index of the considered arm, and $I(x_i, y_i, w)$ is the image intensity at $x_i = x + w \cdot \sin \theta_i + l \cdot \cos \theta_i$, $y_i = y + w \cdot \cos \theta_i + l \cdot \sin \theta_i$, where (x, y) is the center position of the model. $F_l(\mathbf{x})$ describes the sum of intensities inside the Y-feature model, represented by the shaded area in figure 3. The angles of the Y-feature model are determined by connecting the center of the model and three vessels on the boundary. In the case of dark vessel, three valleys that minimize $F_l(\mathbf{x})$ are selected and for bright vessel, three peaks maximizing $F_l(\mathbf{x})$ are considered. In the figure below we illustrate this process on bright and dark vessels in the case of color images and angiograms.

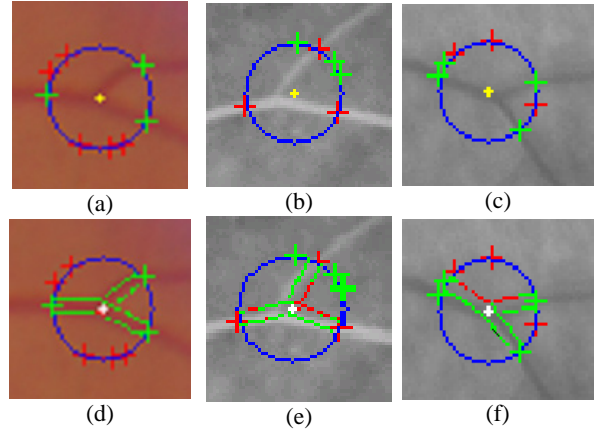


Figure 4. Initial estimation of a bright or dark vessel around the circular boundary. The red cross shows local peaks, and the green cross shows the local valleys characterizing respectively bright and dark vessels. The yellow dot in the middle shows the center position. In (a)-(c) the seed locations detected for bright and dark vessels, (d)-(e) depict the corresponding initialization of the Y-feature model.

3.3. Fitting Y-features

After initializing the position of the Y-feature and the angle of the branches, we fit the articulated Y-features using a gradient descent method. In addition to the constraints defined by equation (2), the gradient value along the boundaries of the vessels is utilized to enhance the accuracy of the estimated Y-feature model. We minimize the following energy:

$$F(\mathbf{x}) = (-1)^m \frac{1}{2} \sum_{i=1}^3 \int_{-W}^W \int_0^L [I(x_i, y_i, w)]^2 dl dw + \frac{1}{2} \sum_{i=1}^3 \sum_{w \in [-W, W]} \int_0^L [G(x_i, y_i, w)]^2 dl \quad (3)$$

where $G(x_i, y_i, w)$ is the gradient value on the boundary, and $m=0$ for bright vessel, $m=1$ for dark vessel.

Additionally, we constrain the angle and width of the branch to be within a specified range of values. The relative angles between the branches of the Y-model are defined by $g_1(\theta)$, $g_2(\theta)$ and $g_3(\theta)$ as follows:

$$\begin{aligned} b_l \leq g_1(\theta) = \theta_2 - \theta_1 \leq b_u, \\ b_l \leq g_2(\theta) = \theta_3 - \theta_2 \leq b_u, \text{ and} \\ b_l \leq g_3(\theta) = \theta_1 - \theta_3 + 2\pi \leq b_u, \end{aligned}$$

where $\theta = (\theta_1, \theta_2, \theta_3)$ and angle boundaries are set empirically: to $b_l = \pi/9, b_u = 10\pi/9$. These bounds were defined after observing that no Y features goes beyond the specified boundary angles in the retinal images. Similarly, the width of each branch is constrained by defining an upper and lower bound on the width:

$$\omega_i \leq w_i \leq \omega_b, i = 1, 2, 3$$

In our experiments, width boundaries are initially set to $\omega_i = 1, \omega_b = 4$. The length of the Y-feature model and the width of vessel boundaries are determined to be proportional to the size of the image. Enforcing these constraints could be achieved using Lagrange multiplier for solving the constrained optimization problem with the above inequalities [1]. Instead, we use a penalization approach using a barrier function. The inequality constraints on the angles θ are translated to the penalty function:

$$B(\theta) = \sum_{j=1}^3 \left(\frac{1}{(g_j(\theta) - b_l)(b_u - g_j(\theta))} \right)^s.$$

Figure 5 shows plots of the barrier function $B(\theta)$ with different values of s , which controls the smoothness of the barrier function.

A similar barrier function is used for the width of the arms, and the complete penalization function considered is:

$$\begin{aligned} B(\theta, \mathbf{w}) = & \sum_{j=1}^3 \left(\frac{1}{(g_j(\theta) - b_l)(b_u - g_j(\theta))} \right)^s \\ & + \sum_{j=1}^3 \left(\frac{1}{(w_j - \omega_l)(\omega_b - w_j)} \right)^s \end{aligned} \quad (4)$$

where $\mathbf{w} = (w_1, w_2, w_3)$. As s increases, the curve becomes steeper near the boundaries. In our experiments we set $s = 1$.

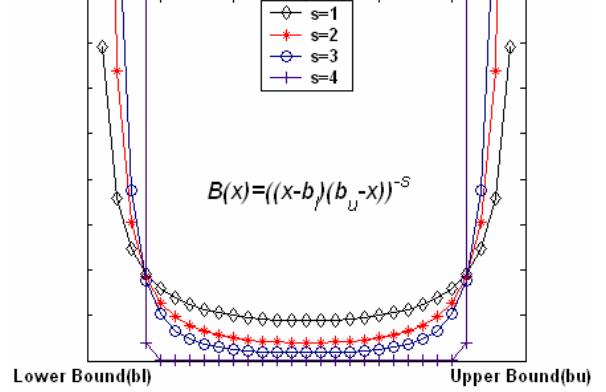


Figure 5: The barrier functions with lower and upper boundary w.r.t. to s . When the value x is closer to the lower or upper bounds, the function penalizes x by associating a large value.

The extraction of Y-features in the image consists of initializing the model using the feature point location and orientations and fitting the articulated Y-model to the image features by minimizing the function:

$$E(\mathbf{x}) = F(\mathbf{x}) + \lambda B(\theta, \mathbf{w}) \quad (5)$$

where λ is the trade-off between the goodness of fit to image features and the constraints on the orientation of the arms and their thickness. The function E is minimized iteratively using a gradient-based approach.

All fitted Y-features do not necessarily correspond to real ramifications of vessels. Indeed many initial Y-features are selected based on whether they have a high response to the directional filters, as described in Section 2. A large number of seed points are considered in order not to miss any real Y-feature in the image. After fitting the articulated model to the selected image regions, we discard extracted Y-feature points for which the boundary of the arms of the articulated model does not lie on strong edge points.

4. Matching and Global Registration

The circulation of the sodium fluorescein dye in the retinal vessels translates into different grey level properties in the color and angiogram images, making the matching of extracted Y-features more challenging. We propose to match extracted Y-feature across modalities and through different phases of the circulation using the local maximization of the mutual information. A RANSAC (Random Sample Consensus) method [6] is used for pairwise registration of images. This however does not provide robust registration of the image sequence, and a global

registration is required. We propose achieving a robust global registration of multimodal frames using a minimum spanning tree.

4.1. Matching Y-features using Mutual Information

Mutual information for a pair of windows \mathbf{z}_A and \mathbf{z}_B is defined by [16]:

$$E_{MI}(\mathbf{z}_A, \mathbf{z}_B) = H(\mathbf{z}_A) + H(\mathbf{z}_B) - H(\mathbf{z}_A, \mathbf{z}_B) \quad (6)$$

where $H(\mathbf{z}) = \int p(\mathbf{z}) \ln p(\mathbf{z}) d\mathbf{z}$ is Shannon entropy of the image window \mathbf{z} , and p is the distribution of the grey levels in the considered window. Equation (6) indicates that the maximization of mutual information is related to the minimization of the joint entropy $H(\mathbf{z}_A, \mathbf{z}_B)$ [12]. We consider the following approximation of the entropy:

$$H(\mathbf{z}) \approx -\frac{1}{N_z} \sum_{z_i \in \mathbf{z}} \ln p(z_i)$$

where N_z is the size of the window \mathbf{z} , and the density function $p(z)$ is estimated based on Parzen Window density estimation. We consider a Gaussian density function for the Parzen window W_p , and the distribution of the grey levels is locally approximated as follows:

$$p(z) \approx \frac{1}{N_p} \sum_{z_j \in W_p} g_\psi(z - z_j)$$

where N_p is the number of sample in the Parzen Window W_p , and $g_\psi(z)$ is the uni- or bi-variate Gaussian density function with diagonal covariance matrix ψ [16]. Now the entropy function becomes:

$$H(\mathbf{z}) \approx -\frac{1}{N_z} \sum_{z_i \in \mathbf{z}} \ln \frac{1}{N_p} \sum_{z_j \in W_p} g_\psi(z_i - z_j) \quad (7)$$

We consider a window enclosing the Y-feature model in the source image is compared with other windows in the target image within a specified neighborhood. Y-features for which the mutual information is maximal among the set of candidates are paired.

4.2. Global Registration

Using matched pairs of Y-features, images are registered using an affine transform. The RANSAC method is used to find the inliers among the matched features. The best three matching pairs are selected to obtain the best affine transform, which minimizes the geometric errors of every match:

$$\mathbf{A}_{best} = \arg \text{Min}_{\mathbf{A}} E_R(\mathbf{A}) = \frac{1}{2} \sum_i \left\{ (\mathbf{x}_i - \mathbf{A}\mathbf{y}_i)^2 + (\mathbf{y}_i - \mathbf{A}^{-1}\mathbf{x}_i)^2 \right\} \quad (8)$$

where \mathbf{x}_i and \mathbf{y}_i are a matching pair and \mathbf{A} is affine transform obtained from selected 3 pairs of Y-features. With the selected affine transform, geometric error of each matching pairs is computed. Based on the error, the outliers of the matching pairs are removed and the inliers are considered for estimating the affine transform.

Image sequences of angiograms can be registered sequentially using a pairwise registration. However, if an image is not correctly registered, this error is propagated to the remaining images. Furthermore, the registration across modalities varies in accuracy according to the phase of circulation of the sodium fluorescein dye in the retinal vessels. Global registration is introduced to automatically reduce the errors of registrations across and within modalities. The global registration is intended to identify the best registration among every pair of images, while minimizing the global registration error.

To address this problem, we consider a graph-based representation, where the nodes correspond to the images to be registered and the edges correspond to pairwise registration of the images. A cost is associated to each edge representing registration error computed by equation (8) obtained by the pairwise registration described above.

We formulate the global registration error problem as finding the minimum spanning tree in this complete and undirected graph. The minimum spanning tree is computed using Prim's algorithm [8]. This will guarantee that the obtained mosaic corresponds to the mosaic with minimal geometric error across features in the images. This approach does not require the tracking of features across the frames, but relies on the pairwise matching of the Y-features. Figure 6 illustrates the difference between pairwise and global registration.

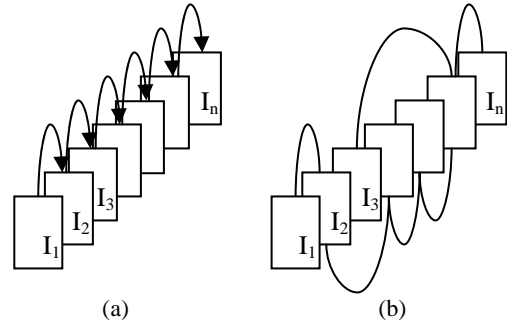


Figure 6. Global registration of frames across modalities using a minimum spanning tree. (a) Pairwise registration of consecutive images (b) Global registration constructed from the minimum spanning tree.

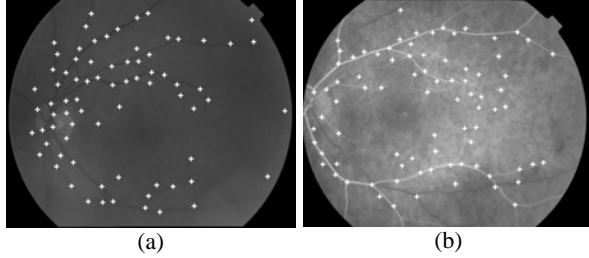


Figure 7: Initial Y-feature position in two images of different modalities. Only the best 100 features are selected.

5. Experimental Results

We conducted experiments on 4 sets of images. Each set corresponds to a clinical case and contains approximately 20 angiograms and one color image. Only the green channel of the color image was considered as it contains the best signal response. Images taken at the end of the circulation of the sodium fluorescein dye in the vessels are very dark with poor contrast. In most of the work dealing with retinal angiogram registration these images are discarded and not registered. Furthermore, in some pathological cases irregular spots with very strong contrast bias the extraction of the Y-features.

We have added, indiscriminately of the image considered, a pre-processing stage based on morphological operator for increasing the accuracy of the Y-feature selection. Morphological operators are applied in order to obtain rectilinear structures in the image. These represent good indication of the presence of a vessel [17]. After opening the image with a linear structuring element with 12 different orientations, the maximum value of the 12 different responses is selected for each pixel. The linear opening and the sum of top-hats remove small isolated spots and enhance vessels detection. To detect dark vessels, the image is inverted before using the same process. Since, we are processing the collection of frames independently of the circulation phase of the dye; images can have both bright and dark vessels. In the experiments described, we have preprocessed all images similarly. Y-features detected from original and preprocessed images are paired for matching and registration of frames. In figure 7 we show the extracted seed points using the PCA analysis of the directional filters.

Fitting was performed based on equation (5). Since the articulated Y-feature has 8 DOF, if we update all 8 parameters at once, the gradient algorithm could be trapped in local minimum. To prevent this, we fixed the three endpoints of the branch and updated only the position and the width of the arms. Once the center

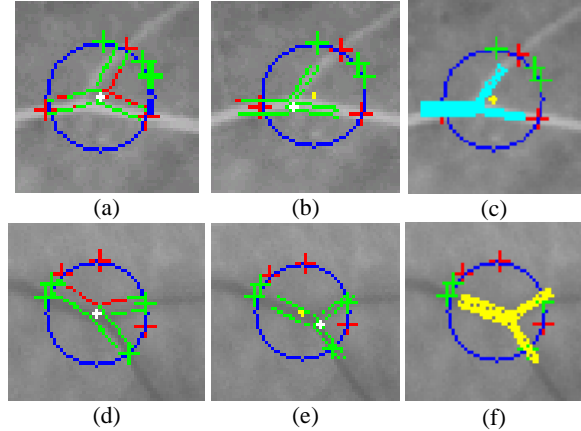


Figure 8. Fitting a Y-feature model to the image data. The yellow and white points correspond respectively to the seed point, and the estimated center point. The green and red crosses indicate respectively local valleys, and peaks in the grey level distribution. (a),(d) Initial Y-feature model of bright or dark vessel. (b),(e) Y-feature model after fitting. (c),(f) Detected Y-features. Every valid Y-feature is classified into bright or dark vessels.

point of the Y-feature converges to a stationary location, angles and widths of branches are updated. The gradient-based minimization scheme is iterated until it reaches a maximum number of iterations, which was set to 25, or the parameters reached stationary values. Figure 8 shows the fitting process. Since the type of vessel (*i.e.* bright/dark) is not characterized by the PCA analysis, the model is fitted twice to detect the Y-feature, first on the dark vessels and second on the bright vessels. Among the two candidates Y-features, the one with a higher gradient value on the boundary is selected.

In the figure 9-(a) and (b) we display the extracted Y-features. The small squares in the image indicate locations selected as an initial Y-feature but were later rejected due to low image gradients along the edges of the Y-feature arms. Figure 9-(c) and (d) show the corresponding inliers pairs after matching and registration. Figure 10 shows the pairwise registration of two images using an affine transform. The global registration was derived using the proposed minimum spanning tree described in Section 4.2. Figure 12 shows the final mosaic image obtained after registering one set of images.

We have conducted an evaluation to quantify the accuracy of the detection of the Y-feature using the proposed articulated model. We have measured the number of detected Y-features, as a variable of the total number of seeds points N_S detected by the PCA-based algorithm. The obtained ROC curve is displayed

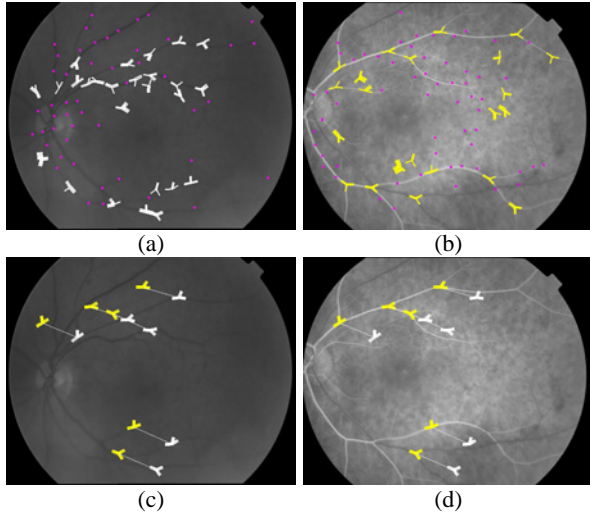


Figure 9. (a) (b) Fitted and validated Y-feature. Squares indicate non-validated Y-features. (c),(d) Matching pairs of Y-features across modalities

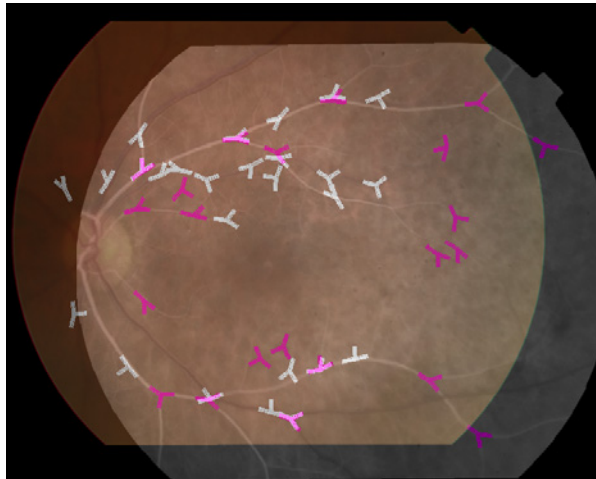


Figure 10. A view of registered images

in figure 11. The ROC curve is saturated at approximately 0.17 false detection rate with more than 0.96 positive detection rate. Ground truth was provided by hand-tagging the location of the Y-features in the image set.

Evaluating the accuracy of the registration across modalities is a difficult task because of a lack of ground truth. We defined the ground truth, by selecting and matching points manually and we have derived the ground truth affine transform matrix. The geometric error of the matching points was calculated from the ground truth affine transform. The average pixel error of the proposed method is 2.6103. This average value was obtained over the whole set of images considered in the 4 set of images (approximately 80 frames).

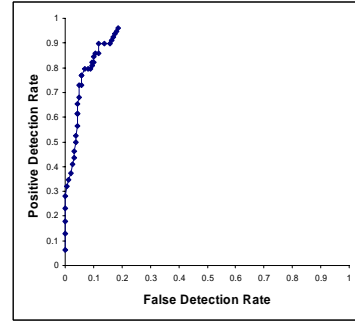


Figure 11: ROC curve of Y-feature detection according to the number of Y-features N_S

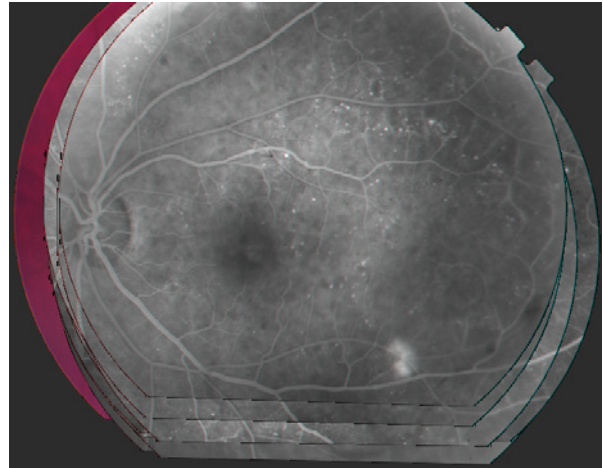


Figure 12. Mosaic image of registered angiograms

We have also compared the proposed approach based on the matching of Y-features to other classically used techniques relying on feature points in the image. In table 1 we show the registration error obtained if we used: only the PCA-based features, pairwise registration of Y- features fitted to image characteristics, and using the global registration method. We notice an improvement of the accuracy by using the proposed minimum spanning tree approach.

To demonstrate the accuracy of fitting process, the result of the pairwise registration using matched seed points is shown in the first column of table 1, and serves as a baseline for comparison.

	Pairwise registration using PCA-based features	Pairwise registration using Y-features	Global registration with fitting
Total Error	4.9313	2.8996	2.6103

Table 1. Comparison of average geometric pixel errors using: pairwise registration of corners, pairwise registration of extracted Y-features, and global registration using Y-features.

6. Conclusion

Extracting Y-features using an articulated model provides robust, accurate and fully automatic registration of multimodal retinal images. The PCA analysis of the directional filter responses provides good estimates of the initial position of Y-features. The fitting of the articulated Y-feature model allows to accurately estimating the position of Y-features in the image, as well as discarding false alarms. Registration of color images and angiograms of the retina using the proposed global registration has demonstrated its performance in various difficult cases with images of low contrast. In addition, all processes were completed without any user interaction, and were fully tested and evaluated on a large number of images of the retina images.

Focus of future research is the construction of the 3D structure of retinal image. This will significantly enhance the ability to detect abnormalities in the retinal surface. Accurate matching pairs from this experiment will provide a solid foundation to estimate robustly the fundamental matrix.

Acknowledgements

This research was partially supported by the National Institutes of Health (NIH) under grant No. R21 EY015914-01, the Doheny Eye Institute, and the James H. Zumberge Faculty Research and Innovation Fund. Its contents are solely the responsibility of the authors and do not necessarily represent the official views of the NIH. We would like to thank Devarshi Shah for participating in this research effort.

References

- [1] D.P. Bertsekas, *Nonlinear Programming*, 2nd ed. Belmont, MA: Athena Scientific, 1999
- [2] A.G. Brown: A survey of Image Registration Techniques; *ACM Computing Surveys*, vol.24, pp.326-276, 1992
- [3] A. Can, H. Shen, J.N. Turner, H.L. Tanenbaum, and B. Roysam, "Rapid automated tracing and feature extraction from live high-resolution retinal fundus images using direct exploratory algorithms", *IEEE Transaction on Information Technology for Biomedicine* **3:2**, pp 125-138, 1999
- [4] A. Can, C.V. Stewart and B. Roysam, "Robust hierarchical algorithm for constructing a mosaic from images of the curved human retina," in *Proc. IEEE Conf. on Computer Vision and Pattern Recognition*, pp. 286-292, June, 1999
- [5] A. Can, C.V. Stewart, B. Roysam, and H.L. Tanenbaum, "A feature-based, robust, hierarchical algorithm for registering pairs of images of the curved human retina," *IEEE Transactions on Pattern Analysis and Machine Intelligence* **24**, 347-364, March 2002
- [6] M.A. Fischler and R.C. Bolles. "Random sample consensus: A paradigm for model fitting with applications to image analysis and automated cartography," *Comm. Assoc. Comp. Mach.*, 24(6): 381-395, 1981
- [7] M. Foracchia, E. Grisan, and A. Ruggeri, "Detection of Optic Disc in Retinal Images by Means of a Geometrical Model of Vessel Structure," *IEEE Transactions on Medical Imaging*, vol 23, no. 10, pp. 1189-1195, October 2004
- [8] H.N. Gabow, Z. Galil, T. Spencer, and R.E. Tarjan, "Efficient algorithms for finding minimum spanning trees in undirected and directed graphs," *Combinatorica*, vol. 6, 1986, pp. 109-122.
- [9] C. Harris and M. Stephens, "A combined corner and edge detector", *Proc. Alvey Vision Conf.*, Univ. Manchester, pp. 147-151, 1988.
- [10] F. Maes, A. Collignon, D. Vandermeulen, G. Marchal, and P. Suetens, "Multimodality image registration by maximization of mutual information," *IEEE Transactions on Medical Imaging*, vol. 16, no. 2, pp. 187-198, April 1997.
- [11] P.M.D.S Pallawala, Wynne Hsu, Mong Li Lee, Kah-Guan Au Eong. Automated Optic Disc Localization and Contour Detection Using Ellipse Fitting and Wavelet Transform, in *8th European Conference on Computer Vision (ECCV)*, Prague, Czech Republic, May 2004
- [12] J.P.W. Pluim, J.B.A.Maintz, M.A.Viergever, "Mutual-information-based registration of medical images: A survey." *IEEE Transactions on Medical Imaging* vol. 22 no. 8 986-1004 August 2003
- [13] C.L. Tsai, C.V. Stewart, H.L. Tanenbaum, and B. Roysam, "Model-based method for improving the accuracy and repeatability of estimating vascular bifurcations and crossovers from retinal fundus images," in *IEEE Transactions on Information Technology in Biomedicine*, Volume 8, Issue 2, Jun 2004 pp.122 - 130
- [14] P.A. Viola and W.M. Wells, III. Alignment by maximization of mutual information. *International Journal of Computer Vision*, 24(2):137-154, September 1997.
- [15] Thomas Walter, Jean-Claude Klein, "Segmentation of Color Fundus Images of the Human Retina: Detection of the Optic Disc and the Vascular Tree Using Morphological Techniques," *ISMDA 2001*: 282-287
- [16] W.M. Wells III, P. Viola, H. Atsumi S. Nakajima, and R. Kikinis, "Multi-modal volume registration by maximization of mutual information," *Medical Image Analysis*, vol. 1, no. 1, pp. 35-51, March 1996.
- [17] F. Zana and J. C. Klein, "Segmentation of Vessel-like Patterns Using Mathematical Morphology and Curvature Evaluation," in *IEEE Transactions on Image Processing*, vol. 10, no. 7, pp. 1010-1019, July 2001.